# Au-Sn alloy phase diagram and properties related to its use as a bonding medium

# Goran S. Matijasevic, Chin C. Lee and Chen Y. Wang

Department of Electrical and Computer Engineering, University of California at Irvine, Irvine, CA 92717 (USA) (Received March 4, 1992; accepted September 7, 1992)

#### Abstract

Au-Sn eutectic alloy has been successfully used in microelectronic packaging for high reliability applications where a hard solder as well as a low processing temperature are required. A new multilayer bonding technology not only has produced nearly perfect bonding but also has reduced the processing temperature even below the eutectic melting point. Knowledge of the different phases of the alloy and their formation, as well as the interdiffusion that occurs, thus becomes important in studying the bonding principle and the long-term reliability. In this paper, we review a large number of publications on the Au-Sn system and summarize the important properties. We hope that this summary would further enhance the development of new Au-Sn bonding methods as a result of an overall understanding of oxidation and diffusion properties.

### 1. Introduction

A semiconductor package plays an important role in electronic products as it serves the purposes of heat dissipation, mechanical support and electrical connection. The integrated circuit chip or die is bonded to the package and the bonding needs to satisfy these purposes. The quality of the die attach is important since unreliable bonding leads to early device failure as a result of inadequate heat dissipation and low mechanical strength. Commonly used die bond media include soft solders, hard solders, and metal-filled epoxies and glass. Hard solders have been used for over 30 years for highly reliable die attach and include eutectic alloys of Au-Si, Au-Ge, and Au-Sn, which have melting temperatures of 363 °C, 361 °C, and 280 °C respectively [1, 2]. Compared with soft solders and epoxies, hard solders have the advantages of very high strength, no thermal fatigue, as well as no outgassing.

Of the three hard solders, the Au-Sn eutectic alloy has the lowest melting temperature and therefore has special use for devices sensitive to high processing temperatures such as GaAs dice [3-8]. The high thermal conductivity of the alloy makes it especially attractive in power amplifier packages which tend to run hot [7]. Successful attachment of large Si dice with Au-Sn alloy has also been demonstrated in spite of the large thermal expansion mismatch [9-11]. Futhermore, this eutectic alloy also has good mechanical properties, *i.e.* high strength and lowest Young's modulus of the hard solders. As well as its use in die bonding, it is thus often used in the electronic industry for tape automated

bonding (TAB) [12], microsensor bonding [13], package lid sealing [14], and attachment of the multilayer ceramic chip carriers to ceramic substrates [15].

Die bonding is carried out by first putting the solder preform on the package. Then the die is placed on the package and the temperature of the solder is raised above its melting point. To prevent oxidation, this is usually carried out in the presence of nitrogen or forming gas flow. Voids in the solder bonds are common [3] and studies have indicated that the cause of voids is the segregation and formation of materials such as oxides and C on the melted solder [4, 16–18]. These materials form a solid film on the molten solder solution, which prevents the solution from producing a bond with the die and the package. The oxide layer which exists on the surface of the as-fabricated solder preform is further enhanced in the bonding process when the preform melts [4, 18]. This results in incomplete wetting of the melted solder along the surfaces that will be attached. A scrubbing motion is often used to break up the surface tension and surface film of the solder [3, 8] but this may lead to additional voiding [5, 6]. Intermetallic formation of AuSn<sub>4</sub> at the solder-metallization interface which can lead to embrittlement and development of stresses when bonding other types of Sn solders (Sn-Pb, Sn-Ag) to Au metallization is not a concern for this eutectic alloy since its main components are Au and Sn [7].

Bonding with an alloy that is slightly different from the eutectic composition [19] raises a need for a better understanding of the reactions present in this alloy as well as the different phases of the system. Successful die attach has recently been achieved using Au/Sn multilayers which were pre-evaporated on the die [20] or on the substrate [21]. Use of pre-deposited layers has the advantages of reducing oxidation and making the die attach medium thinner, down to several microns. This has allowed successful bonding of 100 µm thin dice with 90 µm via holes without cracking [21]. Cracking from via sites due to solder filling of the via holes has been identified as a problem in this type of die using a conventional solder reflow method [3]. Furthermore, multilayer bonding has been accomplished at temperatures below the eutectic temperature [22], thus allowing even lower temperature high reliability bonding often necessary for laser diode dice. This necessitates better knowledge of the interdiffusion mechanism and alloy formation in Au–Sn couples.

# 2. Au-Sn alloy

# 2.1. Phase diagram

The equilibrium phase diagram of the Au-Sn system shown in Fig. 1 [23] represents one of the more compli-

cated and intriguing binary systems. Its complexity is caused by the existence of four different stable intermetallic compounds as well as two eutectic and at least three peritectic points. Over the past century, a great deal of work has been performed to establish the complete Au-Sn phase diagram and to study the characteristics of the many phases identified. The original diagram was given by Vogel in 1905 [24] and later improved on by Hansen [25]. The diagram given in Fig. 1 is that compiled by Okamoto and Massalski [23]. However, the properties and boundaries of several phases are still not completely determined and work is still being conducted on the refinement of the phase diagram, especially in the Au-rich region. Recent work has modified this portion of the phase diagram giving the diagram shown in Fig. 2 [26]. Important properties of the phases themselves are also not well understood.

The terminal solid solution on the left-hand side of the phase diagram has the same crystal structure as Au, f.c.c. This is a substitutional solid solution of Sn in Au,

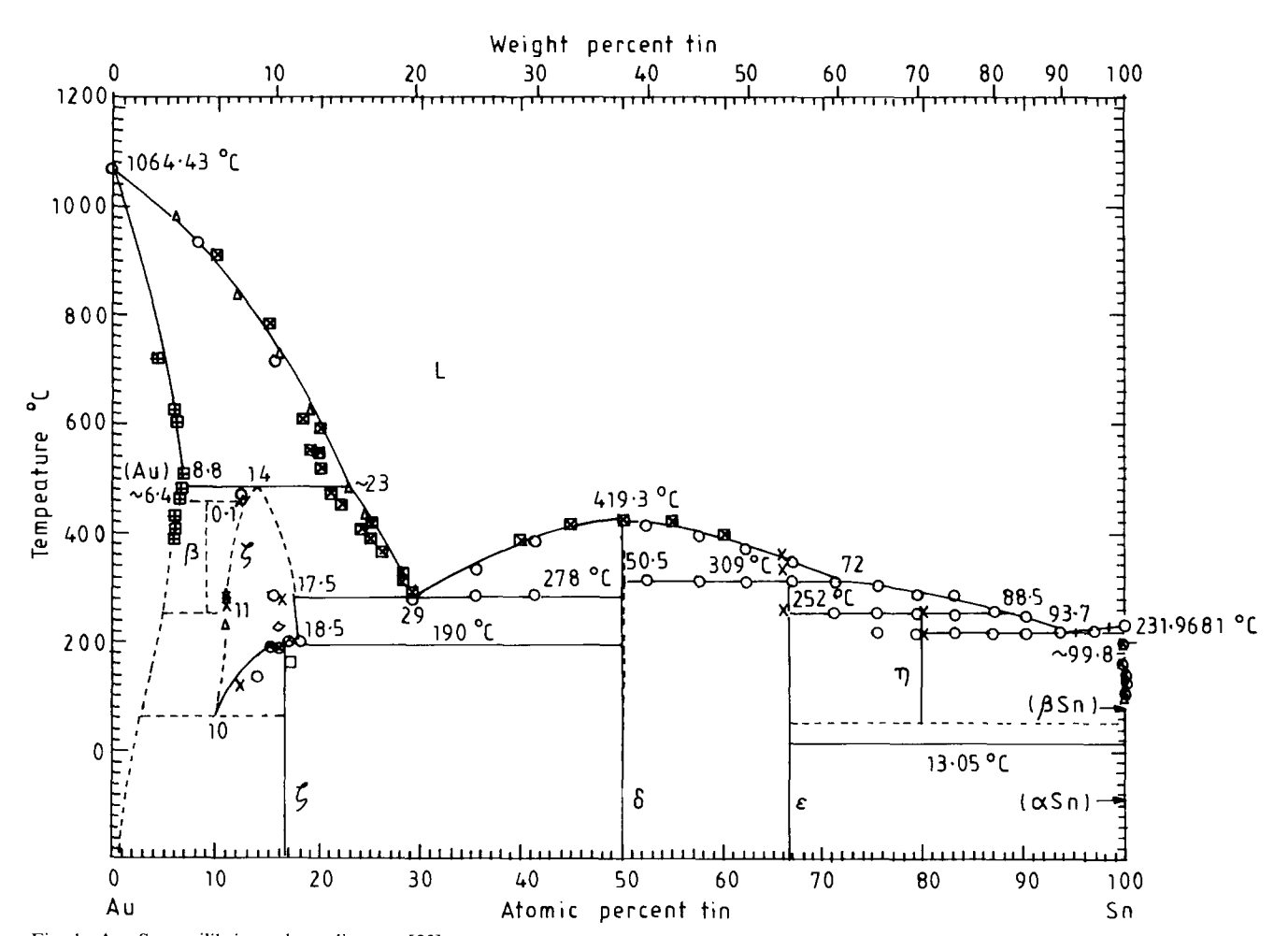


Fig. 1. Au-Sn equilibrium phase diagram [23].

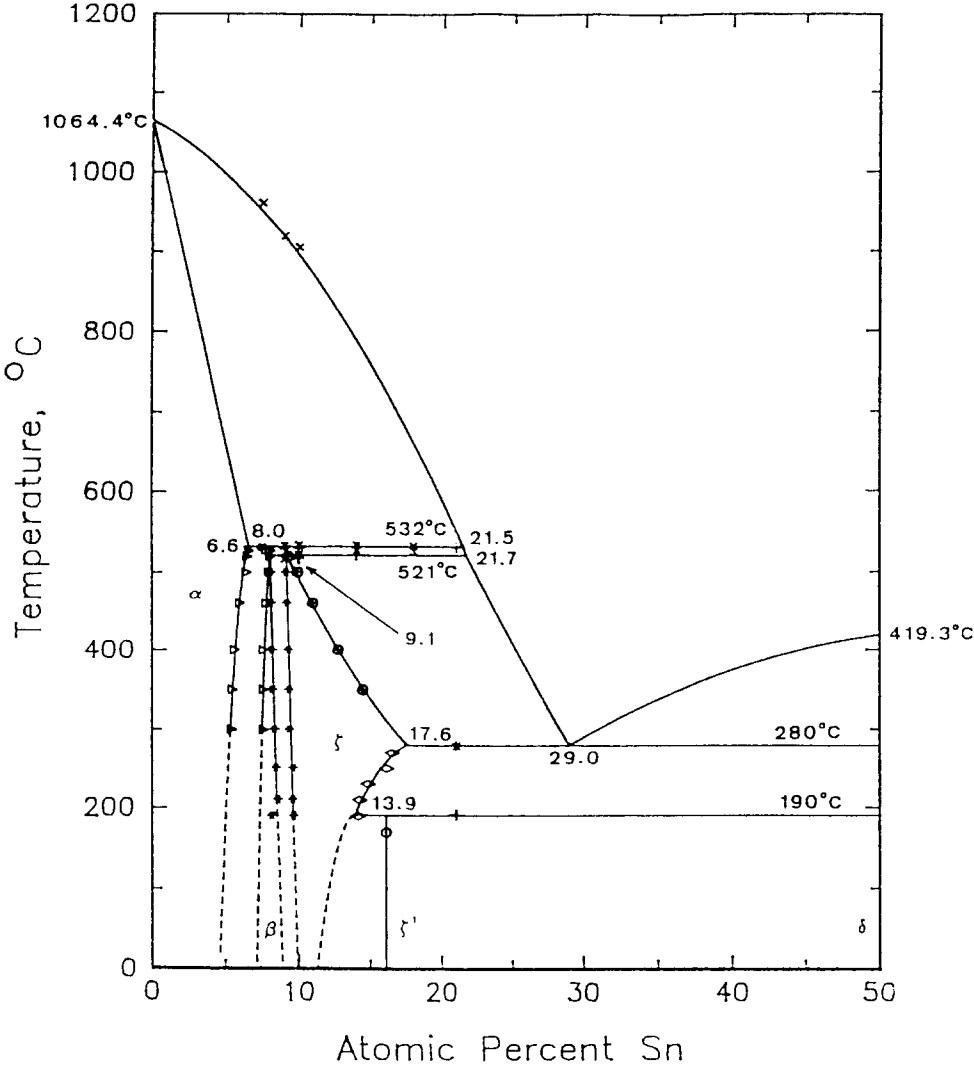


Fig. 2. Au-Sn phase diagram with new measurements for compositions below 50 at.% of Sn [26].

where Sn atoms substitute for Au atoms up to 6.6 at.% in the crystal structure. The substitutional type of replacement of the solid solution is possible here because the atoms are nearly the same size, namely the atomic radius of Au is 1.59 Å, while that of Sn is 1.63 Å, or 2.5% higher [27], which is well below the 15% limit generally considered as the upper limit for the possibility of substitution. The size of the f.c.c. lattice, however, increases as more Sn substitutes the Au atoms. As the Sn content is increased from 0 to 6.6 at.%, the lattice parameter a increases from 4.0784 Å to 4.1053 Å [28]. Correspondingly, the volume per atom increases with increasing Sn concentration in the terminal solution. The extension of this solid solution is limited by the electron concentration. A higher valency of the solute atom causes a smaller maximum solubility of the solute in the terminal solution. Here Sn is tetravalent and the terminal solid solution of Au has a solubility limit of 6.6 at.% of Sn (at 532 °C) [26]. The limit, however, is

also dependent on other factors. One of these is that in an alloy of two elements which differ widely in electrochemical characteristics, one being very electropositive compared with the other (Au is 2.3, Sn 1.8), there is a tendency to form stable intermediate phases or intermetallic compounds at the expense of the primary solid solutions.

As the Sn concentration increases and with temperatures above 532 °C, there is a liquid solution of the Au terminal solid solution. The range of temperatures over which freezing of the liquid solution occurs varies with the composition of the alloy. For pure Au, the melting point is at 1064.43 °C. Addition of Sn to Au lowers the melting point rapidly and the solidus and liquidus meet at two peritectic points and one eutectic point as the melting point drops to 280 °C.

First Au-Sn phase diagrams did not have a peritectic reaction, where a liquid and a solid phase form a second solid phase, in the Au-rich region of the dia-

gram [24]. Later [28], evidence was found for the peritectic reaction  $[L + (Au)] \longleftrightarrow \zeta$  at 498 °C. The temperature of this reaction was then put at 483 °C by Davies and Leach [29]. This has subsequently [30] been divided into two peritectic reactions,  $[L + (Au)] \longleftrightarrow \beta$  at 532 °C and  $[L + \beta] \longleftrightarrow \zeta$  at 519 °C. Newest measurements [26] confirm these two reactions but put the second at 521 °C. Further work is needed for this region of the phase diagram. The two phases brought up here,  $\beta$  and  $\zeta$ , now require some clarification.

The  $\beta$  phase had been assessed to be the Au<sub>10</sub>Sn intermetallic compound, but recent measurements put it at 8.0 at.% Sn [26]. Figure 2 shows that the maximum temperature of such an intermediate phase is 532 °C. It has a double close-packed hexagonal (c.p.h.) stacking structure (such as TiNi<sub>3</sub>) [31]. This phase, originally thought to be stable only above 250 °C, has now been confirmed to exist down to 190 °C [26] and may exist down to room temperature. Further study is needed to elucidate this phase.

The  $\zeta$  phase has been found to extend at least from 9.1 at.% Sn at 521 °C to 17.6 at.% Sn at 280 °C [26]. Its Mg-type c.p.h. lattice changes over this range with lattice constant a increasing and constant c increasing and then decreasing. The net result is an increase in volume per atom as the Sn concentration increases. This increase is at the same rate as the volume increase in the terminal solution when plotted against electron concentration, *i.e.* the ratio of all valency electrons to the number of atoms [32].

The  $\zeta'$  phase is a stable intermetallic compound (Au<sub>5</sub>Sn) with an Sn content of 16.7 at.% [33]. X-ray diffraction study determined that it has a c.p.h. structure with the unit cell of the superstructure having 15 Au and 3 Sn atoms. The homogeneity range of the  $\zeta'$ phase is less than 1 at.% at low temperatures. It exists up to 195 °C where a congruent reaction occurs, forming the  $\zeta$  phase. Measurement of thermophysical properties of Au-Sn alloys indicates transformation near 190 °C involves a volume contraction [34]. In addition to this reaction, another characteristic of the  $\zeta'$  phase is the eutectoid reaction  $\zeta \longleftrightarrow [\zeta' + AuSn]$  in which solid solution  $\zeta$  changes to two different solid solutions at the eutectoid temperature. This reaction occurs at 18.5 at.% Sn and 190 °C [33]. This point is disputed by the findings of Ciulik and Notis [26], shown in Fig. 2, where the eutectoid reaction  $\zeta' \longleftrightarrow [\zeta + AuSn]$  is postulated.

The  $\delta$  phase is the AuSn intermetallic compound with a melting point of 419.3 °C [35]. This silver-gray material is more brittle than Au and harder than either Au or Sn. Unlike compounds with exact ratios of elements, this non-stoichiometric compound has a homogeneity range between 50.0 and 50.5 at.% Sn [36]. The AuSn phase is a subtractional solid solution of a limited range

that can be designated as  $Au_{1-x}Sn$  (0.00  $\le x \le 0.02$ ). X-ray densities calculated with change of composition confirm that the subtraction of Au atoms from the AuSn lattice occurs. The structure of the AuSn lattice is NiAs-type hexagonal with two molecules of AuSn associated with the unit cell [36].

A eutectic reaction where a single liquid solution changes into two entirely solid phases occurs at 29.5 at.% Sn and has the reaction L  $\longleftrightarrow$  [ $\zeta$  + AuSn]. This eutectic alloy has as its constituents the  $\zeta$  and  $\delta$  phases. This is the eutectic point of 20 wt.% Sn and 80 wt.% Au commonly used in bonding and sealing. The eutectic temperature was measured to be 278 °C  $\pm$  2 °C [29], close to original and current measurements of 280 °C [24, 26].

The  $\varepsilon$  phase is the AuSn<sub>2</sub> intermetallic compound. The temperature of the peritectic reaction  $[L + \delta] \longleftrightarrow \varepsilon$  is 309 °C, giving the liquidus composition of 71.3 at.% Sn [24]. The homogeneity range of this phase is very narrow and the crystal structure is orthorhombic c.p.h. [37].

The  $\eta$  phase is the AuSn<sub>4</sub> compound, a centered orthorhombic c.p.h. structure. The homogeneity range of this phase is also very narrow. It was found that thermal and mechanical treatment of AuSn<sub>4</sub> samples has an effect on the crystal structure, causing an interlayer gliding effect between the atomic layers of Au and Sn. This results in decomposition of the AuSn<sub>4</sub> phase and the precipitation of AuSn<sub>2</sub> and  $\beta$ -Sn phases [38, 39]. There is a peritectic reaction  $[L + \varepsilon] \longleftrightarrow \eta$  at 252 °C [24], giving the liquidus composition of about 88.5 at.% Sn.

The second eutectic reaction of this phase diagram  $L \longleftrightarrow [\eta + \beta\text{-Sn}]$  takes place at 93.7 at.% Sn and 217 °C [24]. This eutectic alloy has been studied for its crystallography [40]. Its solidification and morphology were also studied [41]. However, its electrical, mechanical, and thermal properties are unknown.

There are two terminal solid solutions of Sn, metallic (white)  $\beta$ -Sn and semiconducting (gray)  $\alpha$ -Sn. The  $\alpha \longleftrightarrow \beta$  transition in Sn is unique in that the reversible transformation can take place near room temperature and under 1 atm pressure. The allotropic transformation temperature of the Sn phase from the  $\beta$ -Sn b.c.t. structure crystal to the α-Sn diamond cubic-type structure is 13 °C [42]. This is a very slow transformation and seems to be diffusion controlled. This transformation causes the phenomenon known as "tin pest" at prolonged exposures at low temperatures. The reverse  $\alpha \longrightarrow \beta$  transition normally occurs at 20 °C and involves a 21% volume contraction. It has rapid growth and is therefore believed to be martensitic [43]. It is interesting to note that in dilute alloys of Sn-Ge the transformation takes place at higher temperatures [42]. Not enough is understood about this transformation.

Finally, the  $\beta$ -Sn solid solution was found to have a solubility of up to 0.2 at.% Au [44]. The  $\alpha$ -Sn solid solution, on the contrary, has a very limited solid solubility of less than 0.006 at.% Au.

# 2.2. Thermodynamic properties and metastable phases

In order to obtain better understanding of metallurgical phenomena, knowledge of the interatomic bond in the alloys is important. Thermodynamic measurements provide a quantitative measure of changes of bonding energy. Extensive studies have been performed to determine the heat of solution or partial enthalpy of Au in Sn [45-51], integral enthalpy of mixing [50-53], the heat of formation [25, 54, 55], and the heat capacity [51, 56, 57] of the liquid alloy at different concentrations and temperatures. The minimum of the integral enthalpy at 48 at.% Sn indicates strong bonds at this composition [52]. Heat capacity measurements also exhibit maxima at 50 at.% and at about 20 at.% Sn [51, 56]. Calculation of excess entropies reveals deviations at 55 at.% Sn and 25 at.% Sn, indicating formation of clusters in the liquid state in the vicinity of these compositions [58]. Resistivity measurements also exhibit anomalous behavior at 55 and 22 at.% Sn [59]. Measurements of the partial enthalpy of Au give unusual behavior at 28 at.% Sn, indicating a change in the nature of the bonds at this composition [51]. The heat capacity having a minimum at 28 at.% Sn also predicts a bond change [51]. The experimental thermodynamic values were used to calculate the phase diagram [60]. The calculated diagram compares favorably with the experimentally determined diagram. It also has some inconsistencies in the Au-rich region, pointing to the need for further experimental work on this portion.

X-ray diffraction patterns of the liquid alloys were also obtained to determine their structure [61, 62]. Two distinct maxima were found in the intensity peak of the diffraction patterns of the liquid alloy, one corresponding to a random mixture of the component elements, and the other to a close interatomic distance. This indicates that there is strong attraction in the liquid between Au and Sn atoms. This is noted over the entire range of compositions, but most evident at 25 at.% Sn where the interatomic distance 2.85 Å obtained from the diffraction pattern is very close to the Au-Sn distance found in the crystalline compound AuSn of 2.84 Å [61]. This confirms the thermodynamic measurement conclusions that this liquid alloy has very strong bonds. This would lead to the conclusion that the corresponding solid alloy would also exhibit very strong bonding.

Vapor-quenched amorphous alloy films of Au-Sn obtained by condensation on substrates held at 77 K exhibited very good agreement of the interatomic distances with those of the liquid and a strong tendency

for compound formation within their nearest-neighbor arrangements [63, 64]. The values of the interatomic distances of the amorphous alloys at 50 at.% agreed well with that of the AuSn compound, indicating that the short-range order of the amorphous film is close to that of this compound [63]. Compared with alloys in the vicinity, the amorphous—crystalline transformation temperature has a minimum (252 K) at 50 at.% Au concentration. This points to high stability of the AuSn crystalline compound. Resistivity measurements performed during the transformation from the amorphous to the crystalline metallic state also find a gradual decrease in resistivity at the 20 at.% Sn concentration, again indicating that a certain percentage of small crystallites is already present in the amorphous alloy [64].

Several metastable phases have been found for the system by splat cooling, i.e. rapid quenching of an alloy film on substrates at -190 °C. One such phase was the single-phase alloy reported at 92 at.% Sn [65] and another was found at 20.5 at.% Sn [66-68]. The latter is a  $\gamma$  phase with a  $\gamma$ -brass structure and was found to coexist with  $\zeta$  and AuSn. On the basis of the heat of formation, it is believed that this phase is fairly stable with respect to its component elements, but unstable with respect to the competing equilibrium phases. It is asserted that  $\gamma$  phase, which has a heat of formation comparable with those of the stable phases of the system, barely misses formation in the Au-Sn system at equilibrium [67]. More metastable phases were identified by Ishihara et al. [68] including one which melts by a metastable eutectic reaction, 46 °C below the stable eutectic temperature.

# 2.3. Wetting, oxidation, and segregation

The wetting of metal surfaces by molten solder is usually considered solely as an interfacial energy imbalance. However, the intermetallic formation on the wetted surface is often ignored. In fact, calculations show that the driving force for wetting is the reaction between the liquid metal and solid substrate [69]. For multicomponent alloy liquids, the overall driving force for wetting is reaction energies.

Shear viscosity of the Au–Sn eutectic is very low:  $\eta(T_{\rm m}) = 0.9 \,\mathrm{mPa}$  s, where  $T_{\rm m}$  is the melting point of the eutectic (280 °C) [70]. Even though there is association in the alloy liquid, corresponding to a negative enthalpy of mixing, viscosity is very low compared with similar eutectics. It is also lower than that of tin itself (1.85 mPa s).

Keeping these two factors in mind, we should be able to obtain good and easy wetting of the Au-Sn alloy. However, this is often not the case and a scrubbing motion [8] or static pressure [4-6, 10, 11] needs to be used to achieve complete wetting of the surfaces. Good

wetting should be readily achievable since the Au-Sn alloy is being melted and is wetting an Au-coated surface, and since this eutectic has very low viscosity. The explanation lies in the fact that there is an oxide film that is preventing contact with the bonding surface.

Electron spectroscopy for chemical analysis (ESCA) studies performed on eutectic alloy preform before and after melting [4] have shown that there is oxidation of tin as reflected in the shift of the binding energy of Sn electrons. A high concentration of O was found and a conclusion can be drawn that most of the Sn is in oxide form. Apart from the fact that the surface of the melted preform is completely oxidized, significantly smaller Au peaks were identified compared with the eutectic preform scan, indicating a lower Au composition on the surface. In addition to a substantial amount of carbon and oxygen, it was found that the relative concentrations of Sn and Au are not as they should be in the eutectic alloy. The Sn composition was 57.4 at.% rather than the eutectic composition of 29.5 at.%. As the preforms were melted and heated to higher temperature, the Sn composition in the surface layer increased. An increase in the O content was also noted. This observation suggests that, in the melting process, Sn segregates to the surface of the alloy. The Sn was oxidizing on the surface even though the melting process was performed in an H<sub>2</sub> environment. The presence of H<sub>2</sub> has a retarding influence on oxidation, but it seems that even very small partial pressures of O<sub>2</sub> will cause Sn oxidation. The significant amount of C identified was caused by surface contamination. The surface of the samples was not cleaned by any form of ion bombardment so that we would be able to view the natural oxidation of tin and this has left other contamination on the surface.

Other studies of the liquid and solidified Au-Sn alloy reveal similar enrichment of the surface with tin [71, 72]. Ichikawa determined with ESCA an Sn composition of 59 at.% for a sample before melting or oxide cleaning [71]. This is close to the above value of 57.4 at.% [4]. Even samples cleaned with ion bombardment and then melted and solidified still had 42 at.% of Sn on the surface [71]. An oxidized preform that was subsequently melted and re-solidified exhibited an even greater Sn segregation with a concentration of 68.4 at.% [4].

An Auger electron spectroscopy (AES) study of the Au-Sn alloys also found pronounced surface segregation of Sn [72]. These samples were also cleaned of any oxides although this was not easily done. This study found that for the  $\zeta$  phase alloy of 13.3 at.% Sn, the surface layer had a composition of about 57 at.% Sn. Even for a 1 at.% Sn  $\alpha$  solid solution, the surface monolayer had a 54 at.% Sn composition [72]. It is interesting that the  $\delta$  (AuSn) phase, on the contrary, exhibited no Sn segregation, probably because of strong ordering of

this phase. For phase between  $\delta$  and  $\zeta$ , which includes the eutectic alloy, indications are that the surface composition can be determined by using the lever rule applied to the segregated  $\zeta$  phase and the unsegregated  $\delta$  phase. This calculation performed using the  $\zeta$  segregation value given by Overbury and Somorjai [72] gives 54 at.% Sn on the surface of a segregated Au–Sn eutectic alloy. This again agrees well with the 57.5 at.% Sn figure obtained by the ESCA analysis [4].

Sn is expected to segregate to the surface of the Au-Sn alloys since it has a smaller surface free energy than that of Au (0.6 J m<sup>-2</sup> for Sn vs. 1.4 J m<sup>-2</sup> for Au at just below their melting points) [73]. The driving force for segregation is thus the heat of adsorption (also known as heat of segregation) which represents the enthalpy change which results when an atom of Sn in the bulk phase exchanges positions with an atom of Au lying in the surface phase. The general expression is written as [74]

$$\frac{X_{A}^{s}}{X_{B}^{s}} = \frac{X_{A}^{b}}{X_{B}^{b}} \exp\left(-\frac{\Delta H_{a}}{k_{B}T}\right)$$

where  $X_A^s$  and  $X_B^s$  are the equilibrium atom fractions of components A and B in the surface phase,  $X_A^b$  and  $X_B^b$  are the respective atom fractions in the bulk phase and  $\Delta H_a$  is the heat of adsorption. This is the general approach and the model can be expanded to include other effects [74].

The relative sizes of the two atoms play a role as does the strain energy associated with a solute atom in a solid solution of the solvent atom. Alloy parameters such as atomic size ratio, surface tension ratio and bond strength ratio can also be used to predict successfully the segregating component to be Sn [75]. In addition, chemisorption of  $O_2$  tends to increase the surface concentration of Sn because of the higher stability of tin oxide [73, 76].

Looking at the oxidation of the segregated Sn, studies have been performed on Sn oxidation [77, 78], but do not agree on the form of the Sn oxide. Although some found both SnO and SnO<sub>2</sub> [77], others found only SnO<sub>2</sub> [78]. There is a considerable question as to which oxide covers the other if both are present. It is suggested that O penetrates beneath the outermost layers of Sn. The depth of penetration, however, is believed to be small. The oxides cannot be distinguished by ESCA or AES.

A recent study analyzed the form of Sn oxide that formed on Au/Sn composite films [79]. Using ESCA and AES, it was found that Sn segregated to the Au surface and formed an oxide. However, neither of these techniques is capable of distinguishing the oxides, so selected area diffraction was used and it identified SnO<sub>2</sub> as the oxide formed.

Two additional studies were carried out on tin oxidation in an Au-2.0at.%Sn alloy [80, 81]. Even alloys

with such a small amount of Sn had surface layers of Sn oxide. However, both studies found no internal oxidation of the alloy. SnO<sub>2</sub> was identified as the only surface oxide. The thickness of the oxide layer after annealing the alloy at a temperature of 700 °C for 5 min was 0.8 µm [81].

The equilibrium partial pressure  $P_{O_2}$  of oxygen for solder oxidation at a given temperature can be calculated using standard thermodynamic principles [82]:

$$P_{\rm O_2} = \exp\left(\frac{\Delta G_{\rm T}^{\circ}}{RT}\right)$$

where  $\Delta G_{\Gamma}^{\circ}$  is standard free energy change, R is the gas constant, and T is temperature. Using the modified Ellingham diagram [82], the partial pressure of  $O_2$  required for oxidation can be either calculated or directly read from the diagram. For Sn oxidation at  $300\,^{\circ}\mathrm{C}$ , which is the temperature used for melting the Au–Sn eutectic alloy, this calculation gives  $5\times10^{-40}\,\mathrm{atm}$ , indicating that a very small amount of  $O_2$  present will cause Sn oxidation. This explains how the eutectic alloy oxidized even in an  $H_2$ -purged furnace.

# 3. Principle of multilayer bonding and experimental results

### 3.1. Diffusion properties of Au and Sn

On the basis of the phase diagram information, it is seen that all alloys containing 16.7–50 at.% Sn will solidify to form the crystalline structure of the Au compound  $Au_5Sn$  ( $\zeta'$ ) mixed with the AuSn ( $\delta$ ) compound. This is the portion that includes the Au-Sn eutectic alloy. Further on, between 50 and 66.7 at.% Sn, the solid phase will be a mixture of the compounds AuSn and AuSn<sub>2</sub>. From 66.7 to 80 at. % Sn the solidus continues at the temperature level of 252 °C and exhibits a mixture of AuSn<sub>2</sub> and AuSn<sub>4</sub>. Finally, the solidus between 80 and 100 at.% at 217 °C has mixtures of AuSn<sub>4</sub> and Sn. Au-Sn films that were evaporated with different thicknesses of Au and Sn have been shown to form the corresponding compounds given above. The compounds were identified by X-ray diffractometry after several months of room temperature interdiffusion [83]. This has shown that alloys can be formed without melting, but by solid state diffusion over a period of time.

Study of diffusion of Au in Sn single crystals revealed very rapid Au diffusion [84]. This bulk diffusivity was attributed to the interstitial mechanism in which the Au atoms enter into the interstitial positions of the Sn lattice. This is apparently in violation of the atomic radius rule that would necessitate a substitutional solution as described previously. However, the radius of an Sn ion in the lattice is considerably smaller than the

atomic radius, *i.e.* only 0.59 Å [27]. This is only 0.37 of the Au atom radius and thus favorable to interstitial diffusion in Sn. This diffusion is faster by 3–4 orders of magnitude than the self-diffusion of Sn [85].

The topic of diffusion in Au-Sn film couples which consist of thin Au and Sn layers deposited on different substrates has been studied extensively [83, 85–103]. Work has been carried out to determine which diffusion mechanism is responsible for the intermetallic compound formation. With the use of a diffusion marker and depth profiling by Rutherford backscattering spectroscopy, it was found that Au diffuses very rapidly both interstitially and along the grain boundaries of Sn [97]. Au is transported along the grain boundaries into the Sn film, saturating the grain boundaries in the process. With smaller Sn grains, there is greater density of the grain boundaries and, therefore, faster diffusion. This is the reason why Au diffuses faster in thin film couples where Sn is evaporated on top of Au [88, 89]. Since Au has smaller grains than Sn, i.e. 100-500 Å vs. 1000-5000 Å, Sn grown on Au will have a smaller grain size and therefore more grain boundaries than Sn grown on a substrate [89]. From the grain boundaries, Au diffuses into the grains by the interstitial mechanism and is included in the grains by the formation of intermetallic phases. The diffusion along the grain boundary and into the grains is very fast and is actually limited by phase formation [99]. The extrapolated room temperature diffusion rate of Au in Sn is 1.9 × 10<sup>-14</sup> cm<sup>2</sup> s<sup>-1</sup> [100]. For low enough temperature, i.e. below -150 °C, layers will remain as grown [96].

Sn diffusion along Au grain boundaries was also found [94, 96, 98], but it is slower than Au diffusion along the Sn grain boundaries [97]. The possibility of Kirkendall void formation due to grain boundary diffusivity was also investigated [94, 95]. It was found that film thinning occurs around large intermetallic grains [95].

It was found that AuSn compound is the first to form in interdiffusion [89, 91-93]. The formation of the AuSn phase at the interface is in agreement with the Walser and Bene first phase nucleation rule, which states that the first compound nucleated in planar binary reaction couples annealed at low temperatures is the most stable congruently melting compound adjacent to the lowest temperature eutectic on the bulk equilibrium phase diagram [104]. In the Au-Sn phase diagram, the only congruently melting phase is AuSn. In addition to AuSn, some AuSn<sub>4</sub> compound formation at the initial stage has also been observed at the beginning of interdiffusion [93]. While AuSn formation occurs at the interface, AuSn<sub>4</sub> occurs within the Sn film and is due to fast grain boundary diffusion of Au into Sn [97, 99]. Phase formation at later stages of interdiffusion involves the decomposition of one of these phases. If there is a high concentration of Au, the  $AuSn_4$  phase disappears, whereas, if we are dealing with an Sn-rich film couple, AuSn eventually consumes all the Sn and transforms to  $AuSn_2$  and  $AuSn_4$  [93]. The phases formed are in accordance with the phase diagram [88]. In case of a very Au-rich film couple, formation of the  $Au_5Sn$  phase has been reported after prolonged interdiffusion at room temperature [83] or on annealing at higher temperatures [88, 92, 93].

Since AuSn compound formation at the interface was found to be a diffusion-controlled planar growth process [92, 96], the kinetics of phase growth is expressed in terms of the width or thickness W of the AuSn layer as

$$W = (2Kt)^{0.5}$$

where t is time and K is the growth rate constant [91, 99]. The parabolic time dependence of compound formation actually falls somewhat below the  $t^{0.5}$  power law. This is because recrystallization reduces the flux to the interface [91]. The growth rate of AuSn at room temperature was found to be  $3.8 \times 10^{-15}$  cm<sup>2</sup> s<sup>-1</sup> [99].

Compound formation was also noted in the bulk Au-Sn film and bulk Sn/Au film couples except that it was slower than in film couples [102]. In the latter case, it was further slowed by the presence of an Sn oxide layer [105]. For thin film layers, if air was let into the vacuum chamber after evaporation of the Sn, before the Au layer was formed, a layer of Sn oxide was formed also preventing diffusion at low temperatures [87].

Electrochemical deposition of Sn from boiling HCl on Au electrodes was determined to result in the AuSn intermetallic compound [106]. If deposition was continued for longer periods, other intermetallic compounds were found to form as well. Various Au-Sn alloys have been electrodeposited from cyanide baths and investigated with X-ray diffraction [107]. Although a linear relationship was not found between the Sn content in the bath and the Sn content in the alloy formed, a relationship was found between the two that allows formation of a desired alloy. It was also found that the alloy composition of the electrodeposited Au-Sn was shifted to the Sn side in comparison with the alloys at thermal equilibrium, thus exhibiting the ζ phase in the 25-29 at.% range [107].

# 3.2. Multilayer bonding

### 3.2.1. Principle

Au-Sn film couples have been studied mostly as ohmic contacts to semiconductors. They are especially used as low resistance ohmic contacts on GaAs. Generally, these thin films are few hundreds to a few thousands of ångströms thick, but some studies looked at 1 µm thick film couples. Here we examine multilayers for bonding of semiconductor dice.

Diffusion bonding is a joining process in which parts to be bonded are held together with sufficient pressure to allow intimate contact, but not to cause macroscopic deformation. Solid state diffusion will then occur forming a bond between the two surfaces [108]. The parts are sometimes heated to a temperature that ensures faster interdiffusion. Thermocompression bonding used in TAB of very-large-scale integration (VLSI) packages is an example of such a process. If the temperature is raised high enough for one of the components to melt, we have liquid phase bonding. As diffusion in the liquid state is about three orders of magnitude faster than in the solid state, faster joining with less pressure applied is possible with liquid phase bonding.

Recently Au-Sn multilayers were successfully used for the purpose of die bonding. Their use eliminates the need for a preform and allows the deposition of the bonding layer directly onto the die back side or the substrate [20-22]. Sn and Au layers are deposited on the GaAs die as shown in Fig. 3. This is done in succession in vacuum to prevent tin oxidation at the Au-Sn interface. This will allow interdiffusion between the two layers. Since the evaporated layers are made in a proportion that is lacking Au to form the Au-Sn eutectic, interdiffusion will continue with the joined layer of Au. Provided that enough pressure is applied to allow intimate contact between the surfaces and that the temperature is above the melting temperature of Sn, i.e. 232 °C, solid-liquid interdiffusion (SLID) will occur [109]. When Sn melts, it will wet the adjacent Au areas forming Au-Sn alloys and liquid and solid components will interdiffuse. If the temperature is kept above 309 °C, the melting point of the solid solution of  $\delta$  and  $\varepsilon$ , SLID will continue to occur until a uniform layer is obtained. If, on the contrary, the temperature is above 232 °C, but below the eutectic point of 280 °C, liquid phase interdiffusion will stop when  $\varepsilon$  or  $\eta$  is formed (depending on whether the temperature is above or below 252 °C). When the liquid component takes in more Au, it will solidify and then solid state

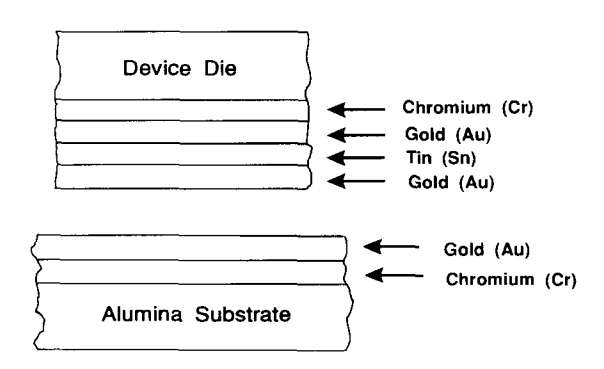


Fig. 3. Multilayer Au-Sn composite structure used for die bonding (not to scale).

diffusion with the remaining Au layer will occur. This will take a longer period of time to complete since solid state diffusion is slower.

## 3.2.2. Experimental procedure and results

The polished side of a 380 µm thick GaAs wafer was deposited with the Cr-Au-Sn-Au composite structure depicted in Fig. 3. The thicknesses of the four layers in the composite are  $0.03 \,\mu\text{m}$ ,  $0.5 \,\mu\text{m}$ ,  $2.25 \,\mu\text{m}$  and 0.75 µm respectively. The surface of the composite is very smooth with a peak roughness less than 0.15 μm. If this composite forms a uniform alloy, it would have 47 at.% Au. After the deposition, the wafer was cleaved into dice 4 mm × 4 mm in size. The substrate used for bonding is 250 µm thick alumina coated with 0.03 µm of Cr and 6.4 µm of Au. The Au layer was produced by sputtering and has an average grain size of about 2 μm. As a result, its surface is not very smooth and has a peak roughness of 0.4 µm. If the Au layer on the substrate and the composite on the GaAs die form a uniform Au-Sn alloy, the alloy would have 84 at.% of Au, which is more than what is needed to result in the Au-Sn eutectic alloy.

The substrates were laid on a graphite boat and the dice were placed on the substrates. To ensure good contact between the dice and the substrates, the dice were held down with 0.276 MPa (40 lbf in<sup>-2</sup>) of static pressure using a mechanical tool. The boat assembly was then loaded into a furnace with a flow of H<sub>2</sub>. The furnace temperature was raised to 310 °C in 8 min and stayed between 310 °C and 320 °C for another 5 min. Afterwards, the boat was pulled out and cooled down to room temperature in 20 min. High quality bondings were consistently obtained.

Figure 4 shows the cross-section of the bonding layer for the die attach carried out at 320 °C. The 8.6  $\mu$ m thickness is less than the total thickness of the original layers of 9.9  $\mu$ m. This is consistent with the volume contraction that the compound formation represents.

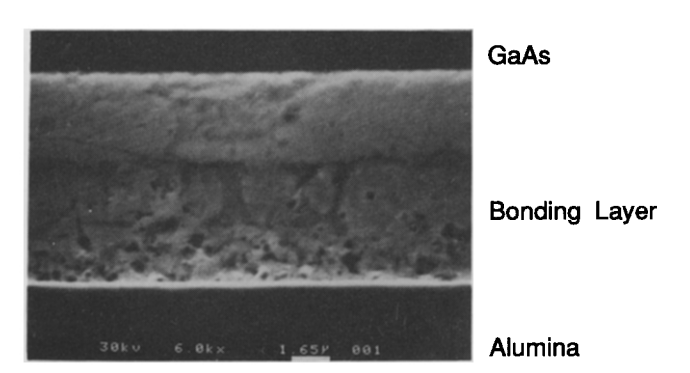


Fig. 4. Scanning electron microscopy (SEM) image of a cross-section of the bonding layer formed by multilayer bonding performed at 320 °C.

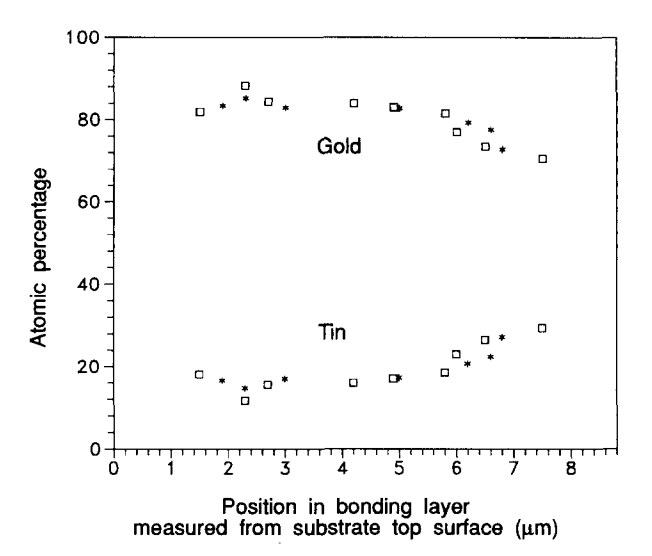


Fig. 5. EDX measurement results along two different traces across the bonding layer given in Fig. 4.

The bonding layer thickness is much less than for the normal die attach achieved with scrubbing (50  $\mu$ m). This is of special concern with via hole die attach where any solder in the via hole can cause die breakage-due to differential thermal expansion [21].

Results of energy-dispersive X-ray (EDX) analysis given in Fig. 5 indicate that Au and Sn composition across the bond are relatively uniform, with the Au concentration being 75–84 at.%, somewhat above the 71 at.% of the eutectic. This is consistent with the design of the multilayer composite with 84 at.% Au and shows that liquid phase bonding resulted in a fairly homogeneous alloy.

Die bonding was also performed at temperatures below the eutectic temperature. This involves solid state diffusion after enough Au is dissolved by the molten Sn to form a solid phase. Bonding was performed with the same structure as above but the Cr-Au-Sn-Au composite thicknesses were 0.07 µm, 0.07 µm, 3.26 µm and 0.19 μm, giving a structure with 11 at.% Au. Together with the Au on the alumina this gives 76 at.% Au. This was then put together as described above with 0.276 MPa (40 lbf in<sup>-2</sup>), but held at only 240 °C for 20 min [110]. Since this is a temperature lower than the melting point of  $\eta$ , solid state diffusion is necessary to complete the bonding. Figure 6 exhibits the cross-section of the bond so obtained. The thickness of the bond is 9.2 µm, compared with 9.5 µm of the original layers, indicating a smaller volume contraction than above.

EDX data on the cross-section, given in Fig. 7, show that there are two layers, one close to the alumina with more than 90 at.% Au and the other beneath the die with around 55 at.% Au. Since the original composite would only give 11 at.% Au, liquid phase diffusion will

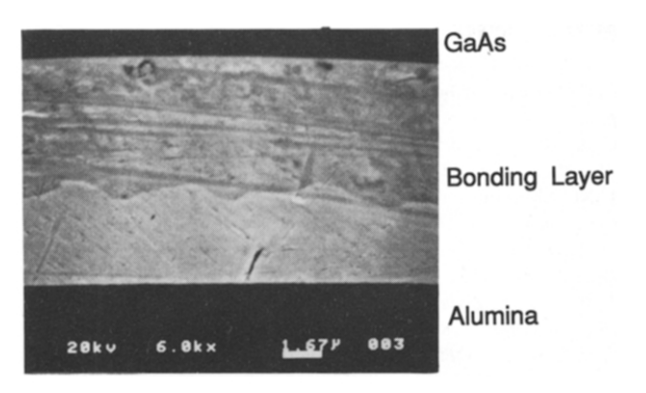


Fig. 6. SEM image of a cross-section of the bonding layer formed by multilayer bonding carried out at 240  $^{\circ}$ C.

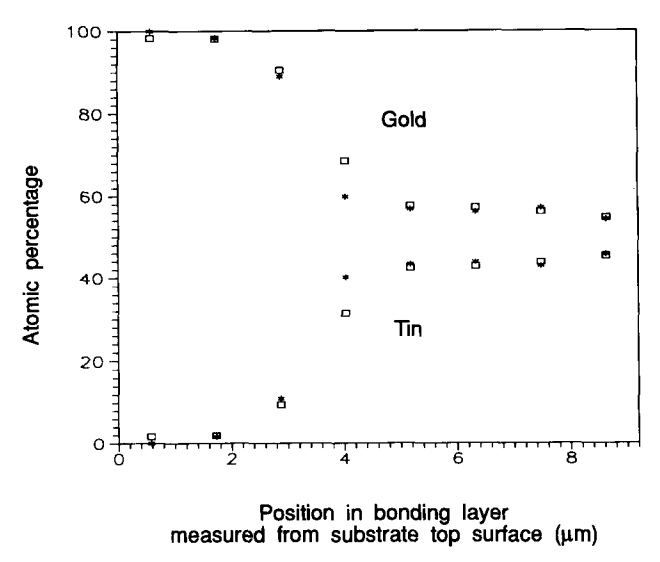
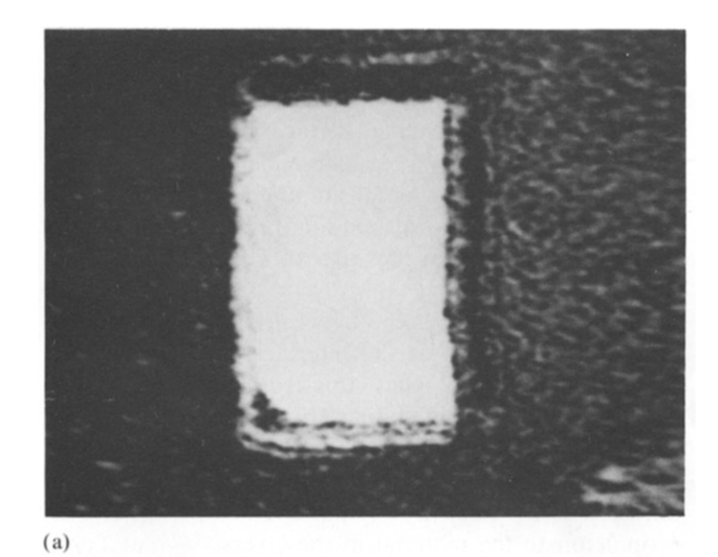


Fig. 7. EDX measurement results along two different traces across the bonding layer given in Fig. 6.

continue until the formation and solidification of AuSn<sub>4</sub>. After the alloy has reached a composition with 20 at.% Au, solid state interdiffusion is necessary for the remainder of the Au to form the Au-rich alloy near the die back side. The solid state diffusion will proceed to form the AuSn compound and with further addition of Au to form the near-eutectic alloy. Even though the bonding layer is not uniform across the whole cross-section as in liquid phase bonding, bonds were shown to be excellent in strength.

To examine the quality of the bonding, transmission scanning acoustic microscopy (SAM) was used to obtain an image of the specimens [111]. Operating at a frequency of 130 mHz, the scanning acoustic microscope has a spatial resolution of 25 µm. The quality of bondings determined by the SAM images has been determined to correlate well with their shear strength [4]. Figure 8(a) exhibits the SAM image of a 2 mm × 3 mm GaAs die bonded at 240 °C, indicating a



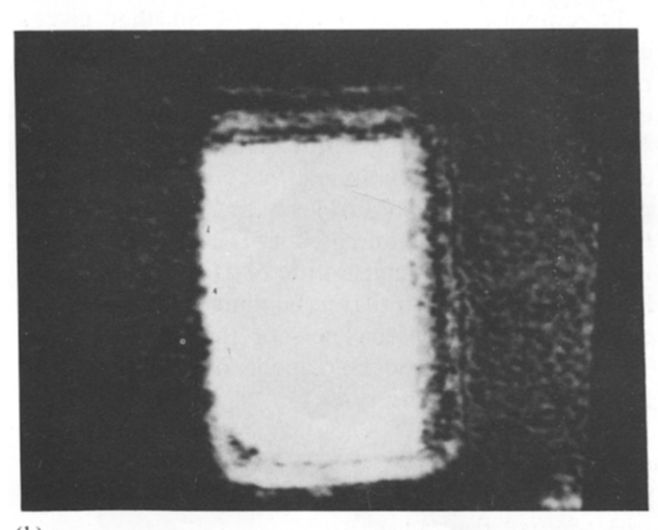


Fig. 8. (a) SAM image of a GaAs die perfectly bonded to an alumina substrate using Au-Sn multilayer bonding performed at 240 °C. (b) SAM image of same specimen as in (a) after post-processing at 250 °C for 20 minutes.

near-perfect bonding. Dark areas in the image indicate voids or defects. No voids larger than 25  $\mu$ m are detected. The bonding was further tested by post-processing at a temperature of 250 °C, with no detrimental effects as seen in Fig. 8(b). This indicates that bonds can be made at a low temperature and subsequently withstand higher temperature use [109].

### 4. Conclusions

Au-Sn eutectic alloy is very useful as a bonding and sealing medium in microelectronic packaging. As a hard solder with a relatively low melting temperature of 280 °C, it has an advantage over other eutectic alloys.

Study of the phase diagram and of the phases formed indicates the possibility of multilayer diffusion bonding.

Segregation of Sn to the surface of the Au-rich alloys, caused by its smaller surface free energy, creates an Sn-rich surface layer. Its subsequent oxidation even in presence of a very small amount of  $O_2$  is a major problem for the preform bonding process. This can be overcome with applied pressure to break up the surface layer.

Interdiffusion studies have revealed the formation of an AuSn compound at the interface. Thermodynamic measurements show that this compound has very strong bonds and that similar strong bonding is exhibited in liquid alloys containing nearly eutectic 25 at.% Sn. Formation of AuSn as a result of solid state diffusion is followed by formation of other phases in proportion to the material in the layers.

Pre-evaporated layers of Au and Sn that give a combined near-eutectic composition have been deposited on the semiconductor die. Interdiffusion was demonstrated successfully even at the relatively thick 10 µm combined layer structure. This was then used as a bonding medium replacing the conventional alloy preform and producing excellent die attach as seen by the scanning acoustic microscope. In addition to offering a lower bonding temperature of 240 °C for sensitive laser diode chips, multilayer bonding can be used to control precisely the thickness of the bonding layer. This allows for new possible applications of Au–Sn in bonding different materials.

## References

- 1 L. Bernstein, Semicond. Prod., 4 (July 1961) 29 32.
- 2 L. Bernstein, Semicond. Prod., 4 (August 1961) 35-39.
- 3 J. S. Pavio, IEEE Trans. Electron Devices, 34 (1987) 2616–2620.
- 4 G. Matijasevic and C. C. Lee, *J. Electron. Mater.*, 18 (1989) 327 337
- 5 G. Matijasevic and C. C. Lee, Proc. 27th Int. Reliability Physics Symp., 1989, IEEE, New York, 1989, pp. 137-140.
- 6 C. C. Lee and G. Matijasevic, IEEE Trans. Compon., Hybrids, Manuf. Technol., 12 (1989) 406-409.
- 7 G. Humpston and D. M. Jacobson, Gold Bull., 22 (1989) 79 91
- 8 M. Nishiguchi, N. Goto and H. Nishizawa, IEEE Trans. Compon., Hybrids, Manuf. Technol., 14 (1991) 523-528.
- 9 T. Uda, Y. Takeo, T. Sato, K. Sahara, S. Kuroda and K. Otsuka, *Proc. 37th IEEE Electronic Components and Technology Conf.*, 1987, IEEE, New York, 1987, pp. 105-109.
- 10 G. Matijasevic, C. Y. Wang and C. C. Lee, *Proc. 40th IEEE Electronic Components and Technology Conf.*, 1990, IEEE, New York, 1990, pp. 786-790.
- 11 G. Matijasevic, C. Y. Wang and C. C. Lee, IEEE Trans. Compon., Hybrids, Manuf. Technol., 13 (1990) 1128-1134.
- 12 T. Kawanobe, K. Miyamoto and M. Hirano, *Proc. 33rd IEEE Electronic Components Conf.*, 1983, IEEE, New York, 1983, pp. 221-226.

- 13 W. H. Ko, J. T. Suminto and G. J. Yeh, In C. D. Fung, P. W. Cheung, W. H. Ko and D. G. Fleming (eds.), *Micromachining and Micropackaging of Transducers*, Elsevier, Amsterdam, 1985, pp. 41–61.
- 14 C. A. Mackay and S. W. Levine, *IEEE Trans. Compon.*, *Hybrids*, *Manuf. Technol.*, 9 (1986) 195-201.
- 15 J. M. Montante and D. R. Kling, Proc. 34th IEEE Electronic Components Conf., 1984, IEEE, New York, 1984, pp. 129-137.
- 16 D. R. Kitchen, *Proc. 18th Int. Reliability Physics Symp.*, 1980, IEEE, New York, 1980, pp. 312–317.
- 17 T. P. Li, E. L. Zigler and D. E. Hillyer, *Proc. 22nd Int. Reliability Physics Symp.*, 1984, IEEE, New York, 1984, pp. 169-174.
- 18 G. Matijasevic, Ph.D. Dissertation, University of California, Irvine, CA, 1991.
- 19 D. D. Zimmerman, Solid State Technol., 15 (January 1972) 44-46.
- C. C. Lee, C. Y. Wang and G. Matijasevic, IEEE Trans. Compon., Hybrids, Manuf. Technol., 14 (1991) 407–412.
- 21 C. Y. Wang and C. C. Lee, *IEEE Trans. Compon.*, *Hybrids*, *Manuf. Technol.*, 14 (1991) 874–878.
- 22 C. C. Lee and C. Y. Wang, *Thin Solid Films*, 208 (1992) 202–209.
- 23 H. Okamoto and T. B. Massalski, In H. Okamoto and T. B. Massalski (eds.), *Phase Diagram of Binary Gold Alloys*, ASM International, Metals Park, OH, 1987, pp. 278-289.
- 24 R. Vogel, Z. Anorg. Chem., 46 (1905) 60-75 (in German).
- 25 M. Hansen, Constitution of Binary Alloys, McGraw-Hill, New York, 1958, pp. 232-234.
- 26 J. Ciulik and M. R. Notis, Proc. 2nd ASM Int. Electronic Materials and Processing Congr., 1989, ASM International, Metals Park, OH, 1989, pp. 57-61.
- 27 W. A. Harrison, *Electron Structure and the Properties of Solids*, Freeman, San Francisco, CA, 1980.
- 28 E. A. Owen and E. A. O. Roberts, *J. Inst. Met.*, 71 (1945) 213–254.
- 29 H. A. Davies and J. S. L. Leach, J. Inst. Met., 96 (1968) 220-221.
- 30 B. Legendre, C. Hancheng, F. Hayes, C. A. Maxwell, D. S. Evans and A. Prince, *Mater. Sci. Technol.*, 3 (1987) 875-876.
- 31 K. Schubert, H. Breimer and R. Goble, *Z. Metallkd.*, *50* (1959) 146–153 (in German).
- 32 T. B. Massalski and H. W. King, Acta Metall., 8 (1960) 677-683.
- 33 K. Osada, S. Yamaguchi and M. Hirabayashi, *Trans. Jpn. Inst. Met.*, 15 (1974) 256-260.
- 34 F. G. Yost, M. M. Karnowski, W. D. Drotning and J. H. Gieske, Metall. Trans. A, 21 (1990) 1885–1889.
- 35 S. Misra, B. W. Howlett and M. B. Bever, *Trans. Metall. Soc. AIME*, 233 (1965) 749-754.
- 36 J.-P. Jan, W. B. Pearson, A. Kjekshus and S. B. Woods, Can. J. Phys., 41 (1963) 2252-2266.
- 37 K. Schubert, U. Rosler, M. Kugle, K. Anderko and L. Harle, Naturwissenschaften, 40 (1953) 437 (in German).
- 38 R. Kubiak, J. Less-Common Met., 80 (1981) P53 P58.
- 39 R. Kubiak and M. Wolcyrz, *J. Less-Common Met.*, 97 (1984) 265-269
- 40 B. Labulle and C. Petipas, Scr. Metall., 12 (1978) 587-590.
- 41 J. J. Favier and M. Turpin, Acta Metall., 27 (1979) 1021-1030.
- 42 R. W. Smith and F. Vnuk, *Mater. Res. Soc. Symp. Proc.*, 21 (1984) 795-801.
- 43 R. W. Smith, J. Less-Common Met., 114 (1986) 69-80.
- 44 E. Jenckel and L. Roth, *Z. Metallkd.*, 30 (1938) 135–144 (in German).
- 45 O. J. Kleppa, J. Am. Chem. Soc., 72 (1950) 3346-3352.
- 46 L. B. Ticknor and M. B Bever, J. Met., 4 (1952) 941-945.
- 47 O. J. Kleppa, J. Phys. Chem., 60 (1956) 842-846.
- 48 R. L. Orr, A. Goldberg and R. Hultgren, *Rev. Sci. Instrum.*, 28 (1957) 767-773.

- 49 R. Boom, Scr. Metall., 8 (1974) 1277-1282.
- 50 R. Hultgren, R. L. Orr, P. D. Anderson and K. K. Kelly, Selected Values of Thermodynamic Properties of Metals and Alloys, Wiley, New York, 1963, pp. 492-499.
- 51 A. K. Jena and J. S. Leach, Acta Metall., 14 (1966) 1595-1605.
- 52 K. Itagaki and A. Yazawa, Trans. Jpn. Inst. Met., 16 (1975) 679-686.
- 53 E. Hayer, K. L. Komarek, J. P. Bros and M. Gaune-Escard, Z. *Metallkd.*, 72 (1981) 109-115.
- 54 O. J. Kleppa, J. Phys. Chem., 60 (1956) 858-863.
- 55 A. K. Jena and M. B. Bever, *Metall. Trans. B*, 10 (1979) 545 549.
- 56 A. Janitsch, K. L. Komarek and J. Mikler, Z. Metallkd., 71 (1980) 629-634.
- 57 P. C. Wallbrecht, R. Blachnik and K. C. Mills, *Thermochim. Acta*, 46 (1981) 167–174.
- 58 A. K. Jena and T. R. Ramachandran, Metall. Trans., 2 (1971) 2958–2960
- 59 A. Roll and E. Uhl, Z. Metallkd., 50 (1959) 159-165.
- 60 P.-Y. Chevalier, *Thermochim. Acta*, 130 (1988) 1-13.
- 61 R. M. Waghorne, V. G. Rivlin and G. I. Williams, *Adv. Phys.*, 16 (1967) 215-222.
- 62 C. N. J. Wagner, N. C. Halder and D. M. North, *Phys. Lett. A*, 25 (1967) 663-664.
- 63 H. Leitz, Z. Phys. B, 40 (1980) 65-70.
- 64 E. Blasberg, D. Korn and H. Pfeifle, *J. Phys. F*, 9 (1979) 1821–1832.
- 65 R. H. Kane, B. C. Giessen and N. J. Grant, Acta Metall., 14 (1966) 605-609.
- 66 B. C. Giessen, Z. Metallkd., 59 (1968) 805-809.
- 67 A. K. Jena, B. C. Giessen and M. B. Bever, *Metall. Trans.*, 4 (1973) 279-281.
- 68 K. N. Ishihara, H. Gohchi and P. H. Shingu, In E. W. Collings and C. C. Koch (eds.), *Undercooled Alloy Phases*, Metallurgical Society, Warrendale, PA, 1986, pp. 49-57.
- 69 F. G. Yost and A. D. Romig, Jr., Mater. Res. Soc. Symp. Proc., 108 (1988) 385–390.
- 70 L. Battezzati and A. L. Greer, Acta Metall., 37 (1989) 1791– 1802.
- 71 T. Ichikawa, Phys. Status Solidi A, 32 (1975) 369-378.
- 72 S. H. Overbury and G. A. Somorjai, *J. Chem. Phys.*, 66 (1977) 3181–3188.
- 73 S. H. Overbury, P. A. Bertrand and G. A. Somorjai, *Chem. Rev.*, 75 (1975) 547–560.
- 74 P. Wynblatt and R. C. Ku, In W. C. Johnson and J. M. Blakely (eds.), *Interfacial Segregation*, American Society for Metals, Metals Park, OH, 1977, pp. 115-136.
- 75 P. A. Dowben, A. H. Miller and R. W. Vook, Gold Bull., 20 (1987) 54-65.
- 76 L. F. Epstein, Ceram. Age, 63(4) (1954) 37-39.
- 77 R. A. Powell, Appl. Surf. Sci., 2 (1979) 397-415.
- 78 D. A. Ashbury and G. B. Hoflund, J. Vac. Sci. Technol. A, 5 (1987) 1132–1135.
- 79 J. Y. Kim and R. E. Hummel, *Phys. Status Solidi A*, 124 (1991) 211–219.
- H. Ohno, Y. Kanzawa, I. Kawashima and N. Shiokawa, J. Dent. Res., 62 (1983) 774-779.

- 81 I. Tanaka, S. Nasu and F. E. Fujita, *J. Jpn. Inst. Met.*, 49 (1985) 701–706 (in Japanese).
- 82 J. Mackowiak, *Physical Chemistry for Metallurgists*, Allen and Unwin, London, 1965.
- 83 V. Simic and Z. Marinkovic, J. Less-Common Met., 51 (1977) 177-179.
- 84 B. F. Dyson, J. Appl. Phys., 37 (1966) 2375-2377.
- 85 K.-N. Tu and R. Rosenberg, *Jpn. J. Appl. Phys.*, *Suppl. 2, Part* 1, (1974) 633-636.
- 86 E. Klokholm and C. Chiou, Acta Metall., 14 (1966) 565-567.
- 87 L. Buene, T. Finstad, K. Rimstad, O. Lonsjo and T. Olsen, *Thin Solid Films*, 34 (1976) 149–152.
- 88 L. Buene, Thin Solid Films, 43 (1977) 285-294.
- 89 L. Buene, Thin Solid Films, 47 (1977) 159-166.
- 90 L. Buene and S.-T. Jacobsen, Phys. Scr., 18 (1978) 397-399.
- 91 J. M. Vandenberg and R. A. Hamm, *Proc. Symp. on Thin Film Interfaces and Interactions*, 1979, Electrochemical Society, Princeton, 1980, pp. 283–289.
- 92 L. Buene, H. Falkenberg-Arell and J. Tafto, Thin Solid Films, 65 (1980) 247–257.
- 93 L. Buene, H. Falkenberg-Arell and J. Tafto, *Thin Solid Films*, 67 (1980) 95-102.
- 94 S. Nakahara and R. J. McCoy, *Thin Solid Films*, 72 (1980) 457-461.
- S. Nakahara and R. J. McCoy, Appl. Phys. Lett., 37 (1980) 42–44.
- 96 M.-G. Barthès and C. Pariset, *Thin Solid Films*, (1981) 305-312
- 97 D. Gregersen, L. Buene, T. Finstad, O. Lonsjo and T. Olsen, Thin Solid Films, 78 (1981) 95-102.
- 98 S. Nakahara, R. J. McCoy, L. Buene and J. M. Vandenberg, *Thin Solid Films*, 84 (1981) 185-196.
- 99 B. Hugsted, L. Buene, T. Finstad, O. Lonsjo and T. Olsen, *Thin Solid Films*, 98 (1982) 81–94.
- 100 C. Chang, T. A. Callcott and E. T. Arakawa, J. Appl. Phys., 53 (1982) 7362–7366.
- 101 S. Varghese, C. I. Muneera and V. Unnikrishnan Nayar, Thin Solid Films, 99 (1983) 385-390.
- 102 Z. Marinkovic and V. Simic, J. Less-Common Met., 115 (1986) 225–234.
- 103 Z. Marinkovic and V. Simic, *Thin Solid Films*, 156 (1988) 105–115.
- 104 R. M. Walser and R. W. Bene, *Appl. Phys. Lett.*, 28 (1976) 624–625.
- 105 H. G. Tompkins, J. Vac. Sci. Technol. A, 2 (1984) 1093-1096.
- 106 T. G. Carver and H. Leidheiser, Jr., J. Electrochem. Soc., 109 (1962) 68-69.
- 107 Y. Tanabe, N. Hasegawa and M. Odaka, J. Met. Soc. Jpn., 34 (1983) 452–459 (in Japanese).
- 108 S. K. Kang and C. G. Woychik, Mater. Res. Soc. Symp. Proc., 108 (1988) 359-364.
- 109 L. Bernstein, J. Electrochem. Soc., 113 (1966) 1282-1288.
- 110 C. Y. Wang and C. C. Lee, Proc. 42nd IEEE Electronic Components and Technology Conf., 1992, IEEE, New York, 1992, pp. 502-507.
- 111 C. C. Lee, G. Matijasevic, X. Cheng and C. S. Tsai, *Thin Solid Films*, 154 (1987) 207–216.